lubricants

MDPI

Article

Metallographic Study and Sliding Wear Optimization of Nano Si_3N_4 Reinforced High-Strength Al Metal Matrix Composites

Ashish Kumar [1], Ravindra Singh Rana [1], Rajesh Purohit [1], Kuldeep K. Saxena [2,*], Jinyang Xu [3,*] and Vinayak Malik [4,5]

[1] Department of Mechanical Engineering, Maulana Azad National Institute of Technology, Bhopal 462003, Madhya Pradesh, India
[2] Department of Mechanical Engineering, GLA University, Mathura 281406, Uttar Pradesh, India
[3] State Key Laboratory of Mechanical System and Vibration, School of Mechanical Engineering, Shanghai Jiao Tong University, Shanghai 200240, China
[4] Department of Mechanical Engineering, KLS Gogte Institute of Technology, Belagavi 590008, Karnataka, India
[5] Department of Mechanical Engineering, Visvevaraya Technological University, Belagavi 590018, Karnataka, India
* Correspondence: saxena0081@gmail.com (K.K.S.); xujinyang@sjtu.edu.cn (J.X.)

Abstract: The strongest among the all-aluminum alloy series is 7xxx due to its unique composition of alloying elements, making it perfect for automotive and aerospace applications. The present research included manufacturing of Si_3N_4 reinforced aluminum alloy (AA) 7068 nanocomposites via stir casting combined with ultrasonication, followed by a bottom pouring technique. The Si_3N_4 reinforcement has been conducted in different fractions (0.5, 1, 1.5, and 2%) by weight. The microstructure characterization of prepared composites was conducted using FESEM, EDS, and elemental mapping. The microstructure of the AA7068 matrix was significantly refined after incorporating Si_3N_4 nanoparticles. The hardness of alloy increased with reinforcement addition and maximized at 1.5 wt.% due to the combined effect of hard Si_3N_4, difference in thermal co-efficient, Hall-Petch, and Orowan strengthening mechanism. The wear resistance significantly increased after incorporating (Si_3N_4)np in the alloy by increased load-bearing capacity and hardness of nanocomposites. The wear of alloy and nanocomposites is mainly due to the adhesion, two-body, and three-body abrasion mechanism. Optimization of wear parameters was completed using the Taguchi approach. The L-25 orthogonal array was selected to perform the wear test, and, later, the ANOVA tool was used to understand the percentage contribution of each factor. The load has the maximum contribution of 65.67%, followed by reinforcement wt.% and sliding distance. Minimum wear loss was noticed when the wear test was conducted on optimum wear parameters (1.5 wt.% reinforcement, 10 N load, and 400 m sliding distance). Hardness and wear behavior were oppositely influenced by the clustering of particles found at 2 wt.% nanocomposites.

Keywords: aluminum metal matrix nanocomposites; dry sliding wear; hardness; optimization

Citation: Kumar, A.; Rana, R.S.; Purohit, R.; Saxena, K.K.; Xu, J.; Malik, V. Metallographic Study and Sliding Wear Optimization of Nano Si_3N_4 Reinforced High-Strength Al Metal Matrix Composites. *Lubricants* **2022**, *10*, 202. https://doi.org/10.3390/lubricants10090202

Received: 18 June 2022
Accepted: 21 August 2022
Published: 28 August 2022

1. Introduction

Aluminum alloy possesses excellent mechanical and physical properties compared to aluminum because of the addition of alloying elements, such as Si, Mg, Zn, Fe, Cu, Ti, etc. The idea of aluminum-based nanocomposite (AMNCs) fabrication offers excellent mechanical, thermal, wear, and surface properties [1–4] compared to traditional metals and Al alloys. This transformation of properties makes them suitable for automotive, marine, structural, and aerospace applications. When aluminum alloy is strengthened with hard ceramic nanoparticles, such as SiC [1,2], Al_2O_3 [3], Si_3N_4 [4] TiB_2 [5], B_4C [6], TiC [7,8], TiO_2 [9], Gr [10,11], CNT [12], fly-ash [13] etc., the developed AMMNCs exhibit superior mechanical and tribological properties. Aluminum alloy is categorized into various groups as per the alloying element content. AA7068 contains Zn as the major element that provides

exceptional mechanical properties, such as high strength, good corrosion resistance, and high workability [9,14], compared to other alloys.

In the evolution of AMNCs, various fabrication techniques are used, such as powder processing [9], pressure infiltration method [15], in situ method [16,17], friction stir processing [18], cold spraying [19,20], and stir casting [21,22]. The powder metallurgy for AMNC production is a cost-consuming method [23]. In contrast, stir casting is prevalent for its benefits, such as low-cost manufacturing, simplicity, and efficiency in turning bulk products into complex near-to-net shapes [24,25]. The surface area and surface energy of nanoparticles are very high, so their tendency toward spontaneous agglomeration becomes higher when they come into contact with the melt. Consequently, it is challenging to distribute nanoparticles homogeneously by the conventional mechanical stirring process [26]. The ultrasonic treatment (UST) is an assuring method to break formed clusters and helps in the homogeneous mixture of fine particles in the continuous matrix phase [27,28]. Yang Y et al. [29] noticed significant dispersion of fine particles in the matrix when ultrasonic energy was transmitted to the melt due to acoustic streaming and ultrasonic cavitation. For higher weight percent, segregation of particles was observed due to the density difference and lower wettability. Ultrasonic-assisted casting with the bottom pouring method could be a game-changer for better distribution of nanoparticles, where the slurry is poured in the mold quickly with the continuation of the stirring process.

Mohanavel V et al. [30] analyzed the tribological behavior and microstructure of Al6351/Si_3N_4 (1, 2, and 3 wt.%) composites. They noticed a decreasing trend in wear rate with increasing Si_3N_4 content. They also observed adhesive wear in the case of alloy and abrasive wear for composites. Alipour M and Eslami [10] investigated the microstructure and wear characteristics of Gr reinforced AA7068 AMNCs; the reinforcement was conducted as 0.1, 0.3, 0.5, 0.7, and 1.0% by weight. They found maximum hardness and uniform distribution at 0.5 wt.%, they performed dry sliding wear tests at different sliding distances, such as 250 m, 500 m, 750 m, 1000 m, and 1500 m, higher wear resistance was observed for nanocomposites compared to alloy, and wear loss increased with sliding distance.

In another wear behavior study of 7068/TiO_2 nanocomposites, microhardness improved after the addition of reinforcement. Delamination and abrasion are the prominent wear mechanisms in AMNCs [9]. Sharma N et al. [31] investigated the tribological behavior of Al6061/Si_3N_4+Gr nanocomposites and optimized the wear response using a genetic algorithm (GA) and response surface method (RSM). They selected four levels of different parameters, such as load (30 N, 40 N, 50 N, 60 N), sliding distance (800 m, 1200 m, 1600 m, 2000 m), and sliding velocity (0.4 m/s, 0.8 m/s, 1.2 m/s, and 1.6 m/s). RSM graphs confirmed the minimum wear loss at a higher reinforcement weight %. The GA response also verified the optimum wear rate achieved at 12% reinforcing content. Micrographs of damaged surfaces are evident for abrasive, fretting, and adhesive wear mechanisms. Ambigai R and Prabhu S [32] studied the tribological behavior of Al/Si_3N_4+Gr composites at 1 km, 2 km, and 3 km sliding distances and 20 N, 30 N, and 40 N loads. They observed that sliding distance significantly contributes 45.63% to the wear rate. At the same time, the contribution of the load was 43.39%, and COF reduced significantly with the addition of Si_3N_4 particles in the Al matrix. Bhuvanesh D and Radhika N [33] conducted a wear analysis of LM25/10 wt.% Si_3N_4 composites by taking three levels of load (10–30 N), sliding speed (1.5–4.5 m/s), and sliding distance (400–1200 m) and found the minimum wear rate of Si_3N_4 reinforced composites at low load, low speed, and high distance. They optimized the wear parameter using the L-27 orthogonal matrix (Taguchi approach); load has the maximum contribution of 25.58% in wear rate, followed by sliding speed (16.28%) and sliding distance (3.49%). Sathish T and Karthick S [34] performed a wear test on 7050/SiC nanocomposites and optimized the wear parameter using the Taguchi approach. They found that the optimum sliding speed, reinforcing content, and sliding distance values are 2 m/s, 6 wt.%, and 1800 m, respectively. Mistry J M and Gohil P P [4] developed Al7075/Si_3N_4 (4, 8, and 12 wt.%) composites through stir casting and examined mechanical and tribological properties. They found the maximum tensile strength at 8 wt.% and

maximum hardness at 12 wt.%, and the microstructure of Al7075/12 wt.% Si_3N_4 composite reveals clustering of particles. They found that the wear resistance increases with Si_3N_4 content due to the formation of the tribo-chemical layer, wear loss, and COF reduction in composites. Kumar GBV et al. [35] characterized Si_3N_4 strengthened Al 6063 composites; reinforcement is conducted in proportions of 0 to 10 wt.% with an interval of 2% via stir casting. They observed that density, tensile strength, and hardness improved with Si_3N_4 weight %, and volumetric wear loss increased with sliding distance and load. The composite exhibits superior mechanical and wear properties at 10 wt.% Si_3N_4 reinforcement in Al 6063 alloy. Rao TB [1] fabricated Al7075/SiC (0.5, 1, 1.5, and 2 wt.%) nanocomposites through stir casting with the ultrasonication technique and performed tensile and wear tests; they found superior wear resistance for composites compared to alloy; the composites' worn surfaces reveal the abrasive wear. They noticed that the developed composites possess superior tensile strength compared to matrix alloy, and the particles were homogeneously dispersed for all compositions. Srivastava N and Chaudhari GP [21] studied the mechanical behavior of Al 6061/Al2O3np composites, Al2O3 added in 1, 2, and 3% by weight, and they found better hardness and strength at 2 wt.%, while both decreased at 3 wt.% due to agglomeration of particles, which was confirmed by microstructure study. The DOE (design of experiments) technique was frequently used by researchers for optimizing the process parameters [36].

After completing the literature survey, it was observed that there is no work reported on the effect of Si_3N_4np reinforcement in high-strength zinc-rich Al alloy (such as AA7068) on microstructural evolution and wear properties. In addition, the rejection and segregation of nanoparticles during mixing and pouring could be minimized using ball milling and stir casting with ultrasonic assistance and the bottom pouring technique (modified stir casting method). The present work included the fabrication of Si_3N_4 reinforced AA7068 nanocomposites using a modified stir casting method. The reinforcement was conducted in the proportion of 0.5, 1, 1.5, and 2% by weight. Field emission scanning electron microscopy (FESEM) and elemental mapping equipped with energy dispersive spectroscopy (EDS) were used to characterize the composites. The sliding wear test was performed on a Pin-on-Disc machine considering various loads, reinforcement weight %, and sliding distances. Later, optimization of wear parameters was completed using the Taguchi statistical approach, and ANOVA was carried out to determine each factor's percentage contribution. A further confirmation test was performed on the optimum set of parameters.

2. Materials and Methods

2.1. Raw Materials and Fabrication

This research used high-strength zinc-rich aluminum alloy (AA7068) as a base material and nano-sized Si_3N_4 as a reinforcing material to develop nanocomposites. Raw aluminum alloy ingots were purchased from M/s Parshwamani Metals, Mumbai, Maharashtra, India; the chemical compositions of the alloy are depicted in Table 1. Silicon nitride (Si_3N_4) was procured from nano research elements, Haryana, India; Figure 1 shows the FESEM, TEM, and EDS of (Si_3N_4)np and the reinforcement properties displayed in Table 2.

Table 1. AA7068 compositions.

Material	Composition (%)
Zn	7.9
Mg	3.1
Cu	2
Fe	0.15
Si	0.12
Al	balance

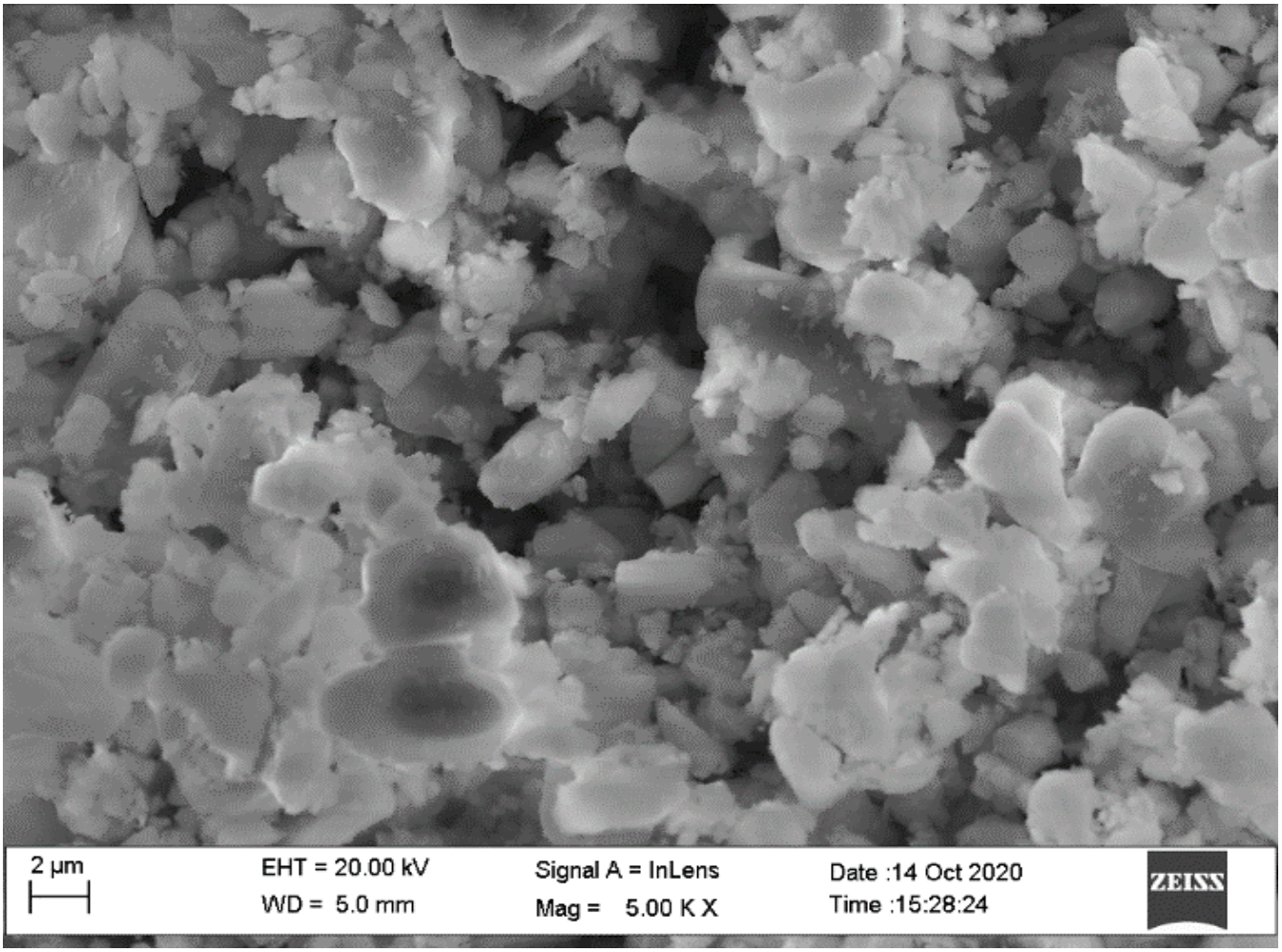

Figure 1. FESEM image of Si_3N_4 nano-powder.

Table 2. Si_3N_4 powder properties.

Parameters	Approximate Range
Size	28.59 nm to 80.13 nm (avg. dia. 4.36 nm)
Molecular weight	140.2833 g/mol
Density	3520 Kg/m^3
Melting point	1900 °C
Color	Off-white
Purity	99.9%

Fabrication of nanocomposites was conducted by novel bottom pouring advanced ultrasonic-assisted stir casting (USC) process; the schematic representation of casting setup is shown in Figure 2. Initially, the mixture of AA7068 powder (approx. 50 µm) and Si_3N_4 nano-powder (avg. diameter 174.36 nm) in a ratio of 1:3 was ball milled for 2 h at 450 rpm. Isopropyl alcohol was used to prevent overheating of milling jars. Prepared milled powder was compacted at room temperature by applying 450 MPa pressure and ready to use in casting. Later, 1 kg of high-strength 7068 alloys was melted at 780 °C, then 1 wt.% coverall was mixed to make slag and impurities free melt. Preheating of permanent mold and compacted milled powder was performed at 450 °C to remove the moisture content. The preheated compacted powder capsules were mixed in molten alloy through mechanical stirring at 500 rpm for 10 min. Ultrasonic waves (2 kHz) were transferred into the slurry for 5 min to break the powder cluster with the help of a 20 mm niobium probe. The processed slurry was bottom-poured in the preheated steel mold with the continuation of the stirring

process. As per ASTM guidelines, specimens for hardness, microstructure, and wear tests were prepared after solidification.

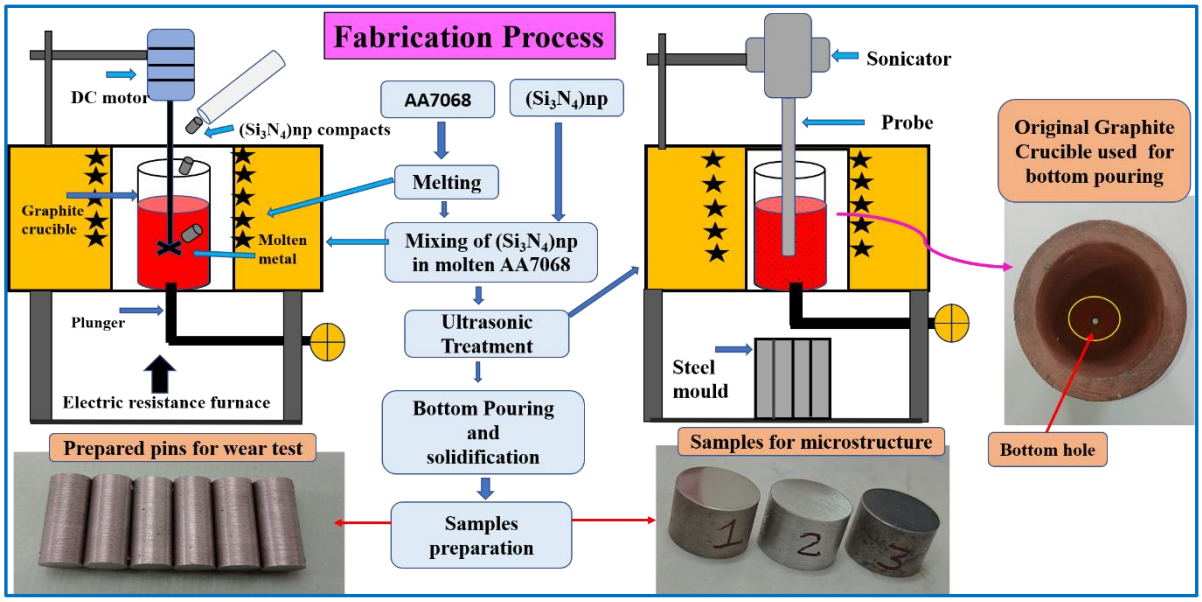

Figure 2. Stir casting setup combined with ultrasonication and bottom pouring technique.

2.2. Characterization Methodology

FESEM was used to analyze the microstructure of specimens, and EDS characterization was carried out at 15 kV accelerating voltage, 4.8 mm working distance using NOVA SEM 450 (IIT Kanpur). Microhardness was measured using an FH-11 series universal hardness tester at the application of 5 N force for 10 s at ambient temperature; the average of ten readings was used for the analysis. Wear tests were performed on a rotary tribometer (DUCOM, Bengaluru, India), shown in Figure 3. For the wear test, cylindrical specimens of 10 mm diameter and 30 mm height were prepared and well-polished to ensure flatness. To determine the weight measurement, the ultrasonic cleaner was used to clean the sample before and after the wear test. An EN-31 steel counter disc (60 mm × 10 mm) with the hardness of 65 HRC was used against composite pins. EN-31steel contained C (0.95–1.2%), Cr (1.2–1.6%), Mn (0.4–0.7%), Si (0.1–0.35%), P (0.04 max), and S (0.05 max). A digital weighing balance (Wensar ISO 9001:2015) with a precision sensitivity of 0.01mg was used for the weight measurement. All the sliding wear tests were performed under dry conditions with varying controlling parameters. Damage surfaces were investigated with SEM (scanning electron microscope).

2.3. Taguchi Modeling

Wear tests of AMNCs were performed on the Pin-on-Disc machine using five levels of applied load (10 N, 20 N, 30 N, 40 N, and 50 N), sliding distance (200 m, 400 m, 600 m, 800 m, and 1000 m), and reinforcement wt.% (0, 0.5, 1, 1.5, 2) at constant sliding velocity of 1.047 m/s and 40 mm track diameter. All the controlling factors with their levels are shown in Table 3. L-25 Taguchi design matrix was selected using Minitab statistical tool 18 (shown in Table 4) to analyze the effect of controlling variables on wear loss for all compositions. The "lower is better" characteristic was used to analyze the wear loss output and SNR (S/N ratio). The relative equation for SNR is given below:

$$S/N = -10Log\ \frac{1}{n}\left(\sum_{i=1}^{n} {y_i}^2\right) \quad (1)$$

where S/N is a ratio of signal to noise, n is the number of repetitions, and y_i is the output value (wear loss) in experiment number i. SNR is calculated for each experimental run with

their respective set of variables. The Taguchi design analysis used a general linear model to obtain the ANOVA (analysis of variance) results and determine each factor's contribution (%) to wear loss. Regression modeling was used to obtain an approximate mathematical equation where wear loss directly depends on other controlling factors.

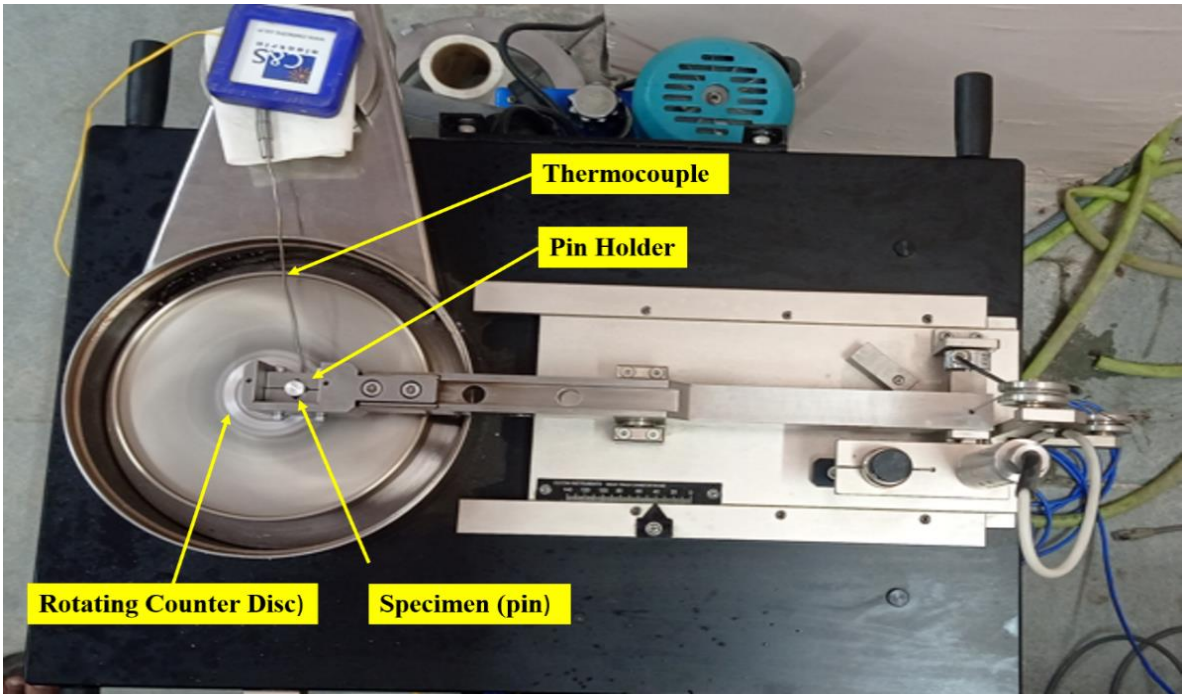

Figure 3. Rotary tribometer (top view).

Table 3. Process variables and their levels.

Factors	L-1	L-2	L-3	L-4	L-5
Reinforcement Wt.%	0	0.5	1	1.5	2
Load (N)	10	20	30	40	50
Sliding distance (m)	200	400	600	800	1000

Table 4. L25 Taguchi design matrix and outcomes.

				Wear Loss (mg)			
Exp. No.	Reinforcement wt.%	Normal Load (N)	Sliding Distance (m)	Experimental	Predicted	% Error	SNR
1	0.0	10	200	5.50	5.14	6.50	−14.8073
2	0.0	20	400	6.89	6.42	6.83	−16.7644
3	0.0	30	600	8.20	7.84	4.42	−18.2763
4	0.0	40	800	9.60	9.40	2.12	−19.6454
5	0.0	50	1000	11.10	11.10	0.02	−20.9065
6	0.5	10	400	4.40	4.41	−0.19	−12.8691
7	0.5	20	600	5.60	5.60	0.07	−14.9638
8	0.5	30	800	7.30	6.92	5.14	−17.2665
9	0.5	40	1000	8.30	8.39	−1.14	−18.3816
10	0.5	50	200	9.20	9.80	−6.57	−19.2758
11	1.0	10	600	3.30	3.73	−13.06	−10.3703
12	1.0	20	800	4.50	4.83	−7.31	−13.0643
13	1.0	30	1000	5.90	6.07	−2.85	−15.4170
14	1.0	40	200	7.20	7.28	−1.05	−17.1466

Table 4. *Cont.*

Exp. No.	Reinforcement wt.%	Normal Load (N)	Sliding Distance (m)	Wear Loss (mg)			
				Experimental	Predicted	% Error	SNR
15	1.0	50	400	8.90	8.78	1.34	−18.9878
16	1.5	10	800	2.82	3.11	−15.19	−8.6273
17	1.5	20	1000	3.80	4.12	−8.39	−11.5957
18	1.5	30	200	4.70	5.12	−8.99	−13.4420
19	1.5	40	400	5.80	6.40	−10.29	−15.2686
20	1.5	50	600	7.40	7.81	−5.58	−17.3846
21	2.0	10	1000	2.90	2.55	12.22	−9.2480
22	2.0	20	200	3.80	3.35	11.93	−11.5957
23	2.0	30	400	4.40	4.39	0.22	−12.8691
24	2.0	40	600	6.30	5.58	11.50	−15.9868
25	2.0	50	800	7.50	6.90	7.98	−17.5012

3. Results and Discussion

3.1. Microstructural Developments

Figure 4a–e shows the microstructure of as-cast alloy and nanocomposites obtained from FESEM. Coarse asymmetric and columnar grains were observed in the monolithic α-Al alloy (shown in Figure 4a). The grain size of α-Al dendrites significantly decreased, and columnar to equiaxed microstructure conversion was noticed after addition of nano Si_3N_4 reinforcement. Apparently, new grain boundaries formed in AMNNCs with Si_3N_4 incorporation; the increased refinement of grains was noticed with increasing reinforcement from 0.5 to 2.0 wt.% (Figure 4a–e). The surface area and surface energy increase with a decrease in size; due to high surface area, nanoparticles form clusters spontaneously when they contact the secondary molten phase. Agglomeration of nanoparticles and porosity observed in the microstructure of nanocomposite contains 2 wt.% Si_3N_4 (shown in Figure 4e). The presence of Si_3N_4 in grain boundaries and grains was identified from the microstructure of AMNCs.

Figure 5 represents the SEM image of the as-cast 7068 aluminum alloy, α-Al, and η-$MgZn_2$ eutectic phase observed in micrographs. EDS confirmed the existence of the intermetallic $MgZn_2$ phase, which reveals that the Zn and Mg contents are more prominent than other alloying elements. Table 5 shows the EDS quantification of nanocomposites containing 0.5, 1, 1.5, and 2 wt.% Si_3N_4. The location (marked as 1, 2, 3, and 4) where EDS was carried out is shown in Figure 6. The EDS spectrum confirmed the presence of Si and N with increasing content from 0.5 to 2 wt.% Si_3N_4 nanocomposites.

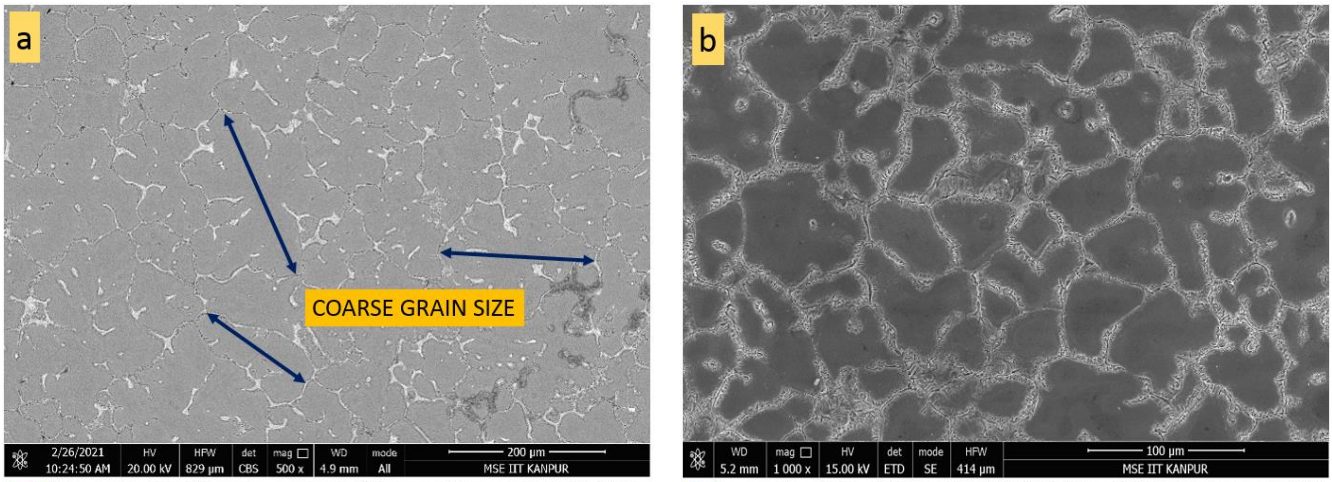

Figure 4. *Cont.*

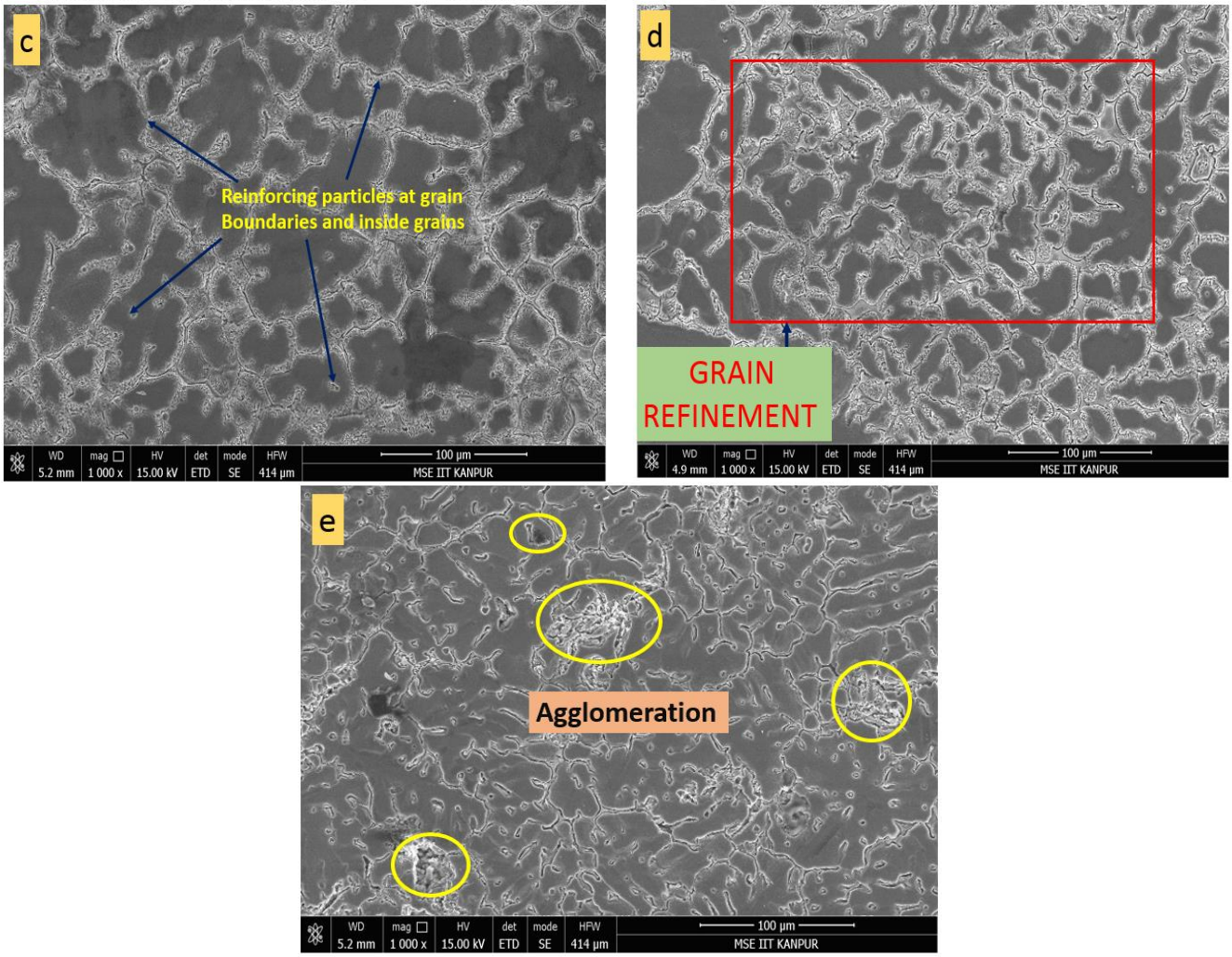

Figure 4. FESEM images of 7068 alloy and its nanocomposites: (**a**) pure alloy; (**b**) with 0.5 wt.% Si_3N_4; (**c**) with 1.0 wt.% Si_3N_4; (**d**) with 1.5 wt.% Si_3N_4; (**e**) with 2.0 wt.% Si_3N_4.

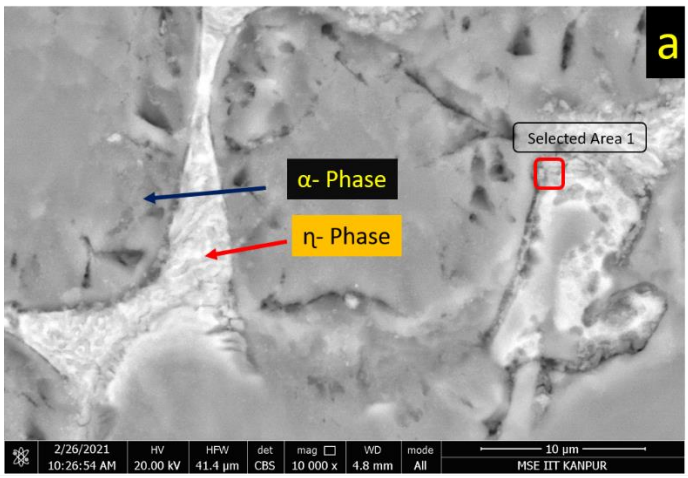

Figure 5. *Cont.*

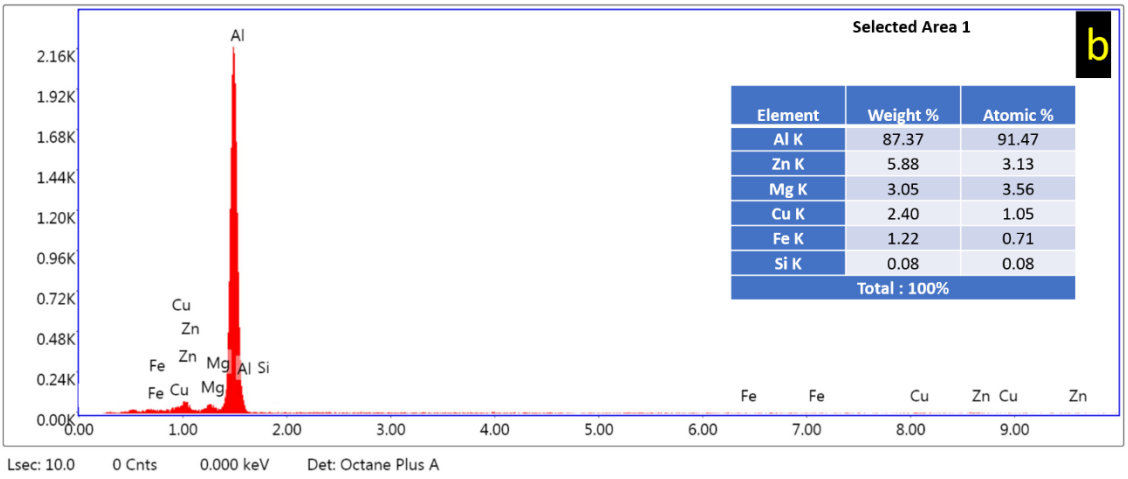

Figure 5. (**a**) Microstructure of AA7068 alloy; (**b**) EDS spectrum of A7068 alloy.

Table 5. EDS quantification for nanocomposites.

	AA7068/0.5 wt.% Si_3N_4 Location (1)		AA7068/1.0 wt.% Si_3N_4 Location (2)		AA7068/1.5 wt.% Si_3N_4 Location (3)		AA7068/2.0 wt.% Si_3N_4 Location (4)	
Elements	**Weight %**	**Atomic %**	**Weight %**	**Atomic %**	**Weight %**	**Atomic %**	**Weight %**	**Atomic %**
N K	0.61	1.24	1.15	2.29	1.74	3.51	2.37	4.81
Mg K	4.22	4.92	3.00	3.46	2.78	3.22	2.80	3.28
Al K	84.98	89.21	86.89	90.18	84.32	88.22	81.86	86.31
Si K	0.03	0.03	0.07	0.07	0.16	0.16	0.18	0.18
Fe K	1.52	0.77	1.41	0.71	2.10	1.06	1.80	0.91
Cu K	1.97	0.88	2.13	0.94	3.60	1.60	4.45	1.99
Zn K	6.67	2.89	5.35	2.29	5.29	2.28	6.84	2.97
	Total = 100%		Total = 100%		Total = 100%		Total = 100%	

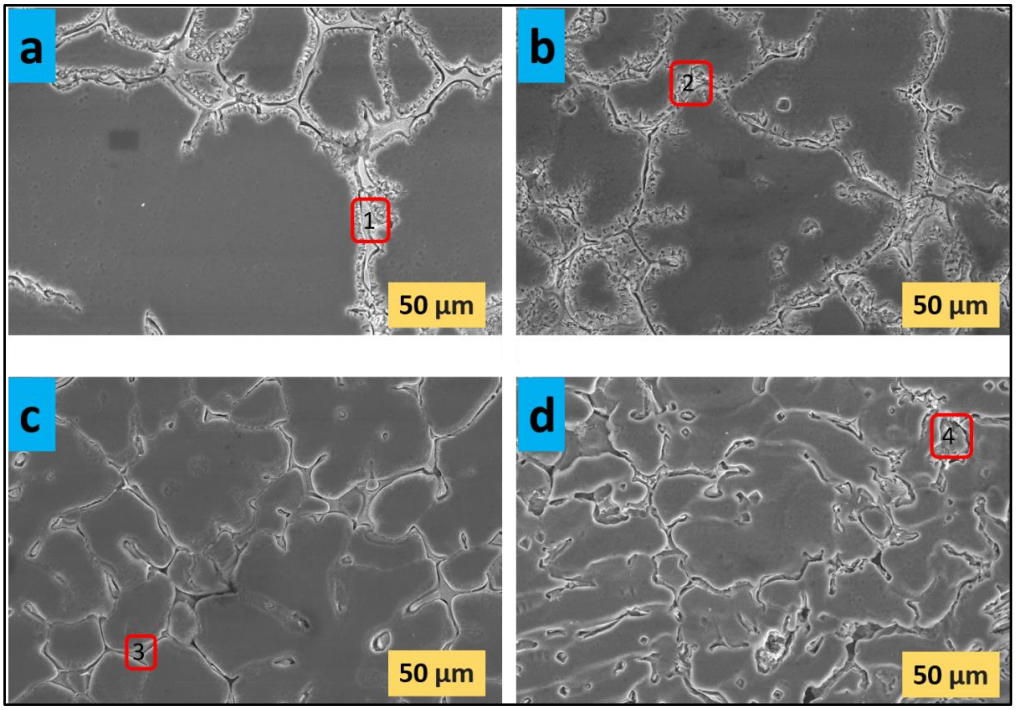

Figure 6. High magnification FESEM of AA7068/Si_3N_4 nanocomposites: (**a**) with 0.5% Si_3N_4; (**b**) with 1.0% Si_3N_4; (**c**) with 1.5% Si_3N_4; (**d**) with 2.0% Si_3N_4.

3.2. X-ray Diffraction (XRD) Analysis

XRD analysis of AA7068 and nanocomposites (from 0.5–2.0 wt.% Si_3N_4) is shown in Figure 7. Al and $MgZn_2$ phases were observed in AA7068, whereas Al, Si_3N_4, and $MgZn_2$ phases were noticed in nanocomposites. For AA7068 alloy, peaks have been obtained in the 2θ span ranging from 20 to 80, and the peaks at 2θ of 39.45°, 45.67°, 65.88°, and 79.76° belong to pure Al, and the peaks at 2θ of 37.31°, 40.98°, and 44.67° belong to $MgZn_2$, and the other remaining minor peaks are attributed to impurity. Similarly, for 2 wt.% nanocomposites, the peaks at 2θ of 39.02°, 45.21°, 65.50°, and 78.52° belong to pure Al, and the peaks at 2θ of 37.25°, 41.08°, and 44.35° belong to $MgZn_2$, and the peaks 2θ of 32.39°, 35.83°, 37.39°, 42.46°, 50.76°, 56.81°, and 74.61° belong to Si_3N_4. It is noticed that the peaks of Al are clearly shown at near 2θ angle of 39°, 45°, 65°, 79°, and the peak of $MgZn_2$ is observed near 2θ angle of 32°, 35°, and 37°.

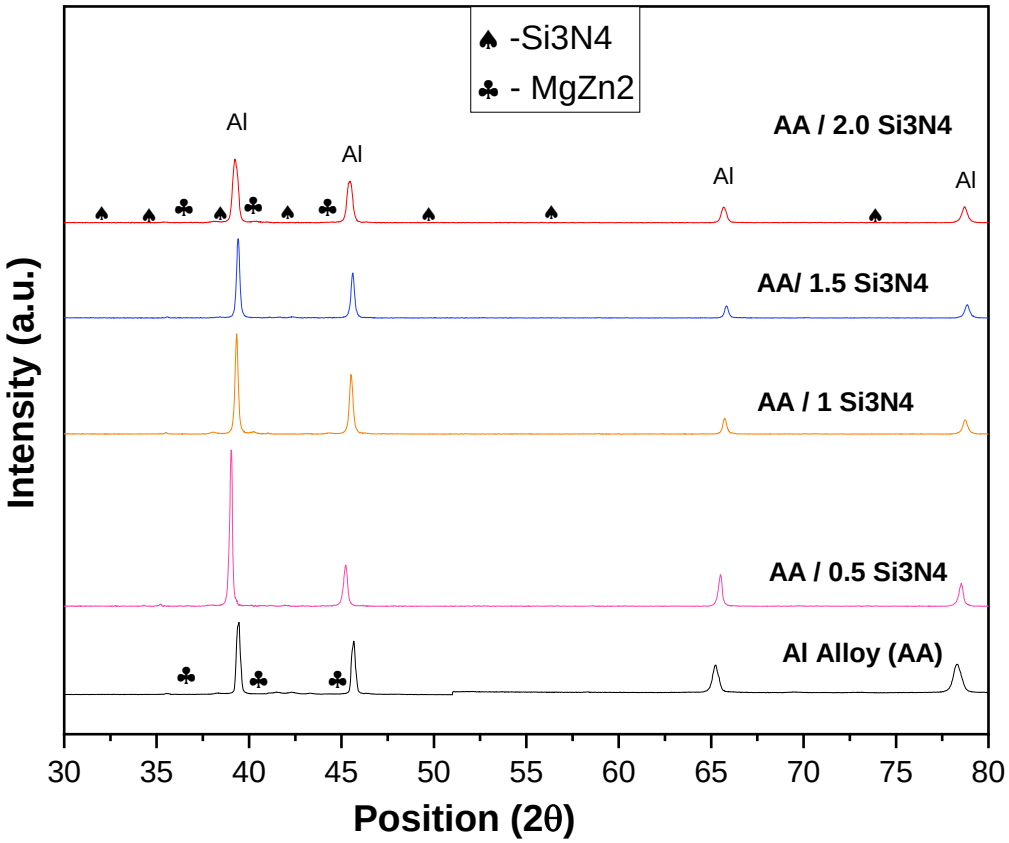

Figure 7. XRD of alloy and nanocomposites.

3.3. Micro Hardness and Porosity

The Vicker hardness of alloy and nanocomposites is shown in Figure 8a. Significant improvement in hardness of nanocomposites was observed due to the collaborated effect of nano Si_3N_4 incorporation, the difference between thermal expansion coefficient (CTE) of alloy and Si_3N_4, and Orowan strengthening. The improvement in hardness was noticed up to 1.5 wt.%. It reduces for 2 wt.% due to the agglomeration of nanoparticles. Microhardness of all compositions was observed by taking the average of 10 indentation values at different locations. The distribution of Si_3N_4 nanoparticles in AA7068 is uniform for 0.5, 1.0, and 1.5 wt.% compared to 2 wt.%. Clustering of particles was observed for AA7068/2wt.% nanocomposites, so the average indentation value for 2 wt.% was calculated as lower due to the uneven distribution of hard Si_3N_4 particles.

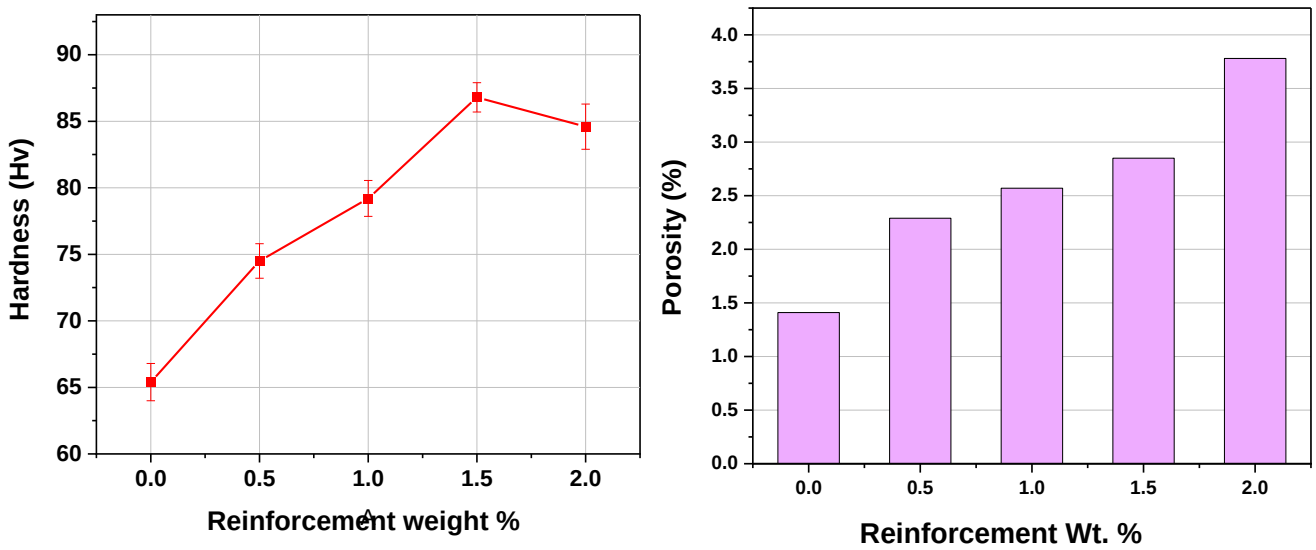

(**a**) (**b**)

Figure 8. (**a**) Hardness of alloy and nanocomposites; (**b**) porosity content (%) of alloy and nanocomposites.

The hardness of the alloy significantly increased by 32.72% with the addition of 1.5 wt.% Si_3N_4. Srivastava N and Chaudhari GP [21] also noticed a similar reduction in hardness of Al 6061/Al_2O_3 composites at higher wt.% due to the clustering of alumina particles.

Figure 8b represents the porosity content (%) of 7068 Al alloy and fabricated nanocomposites. It is observed that the void content increases with reinforcement content from 0.5 to 2 wt.%. The porosity increment is attributed to presented micro air gaps between nanoparticle clusters and air entrapment during the mechanical stirring [3]. The high surface energy and surface area of nanoparticles are responsible for the clustering at different locations. These clusters are broken when ultrasonic treatment is provided to the mixture by the effect of acoustic streaming and cavitation [7]. The trapped air increases the porosity, so the void content increases with reinforcement.

3.4. SNR Analysis

The SNR analysis confirmed the impact of controlling parameters (reinforcement wt.%, normal load, and sliding distance) on wear loss. The highest signal-to-noise ratio value with a set of controlling variables provides the optimum output. The influence of each parameter on wear loss can be quantified by the gap between the upper and lower values of the mean SN ratio. The higher the gap between the mean of SNR, the most impactful would be the variable. Table 6 represents the impact of controlling variables on wear loss. The rating of variables discloses that normal load and wt.% is the leading factor influencing the wear loss, while sliding distance has the minimum influence, so it ranked last.

Table 6. Response table for means.

Level	Reinforcement wt.%	Normal Load (N)	Sliding Distance (m)
1	8.258	3.760	6.080
2	6.960	4.918	6.078
3	5.960	6.100	6.160
4	4.880	7.440	6.320
5	4.980	8.820	6.400
Delta	3.378	5.060	0.322
Rank	2	1	3

Figure 9a,b represents the MEP (main effect plot) for experimental controlling factors on wear loss. Figure 9a depicts the impact of observed experimental factors (reinforcement

wt.%, normal load, and sliding speed) on wear rate. The SNR mean values deviated from the horizontal line for average load and formed a steeper connected line that significantly impacted the wear loss. The slope of the SNR means sharply decreases at 2 wt.% and confirms the increment in wear loss compared to 1.5 wt.% due to higher agglomeration of reinforcing particles. The values of the SNR means are much closer to the horizontal line in the case of sliding speed, indicating the least influencing factor.

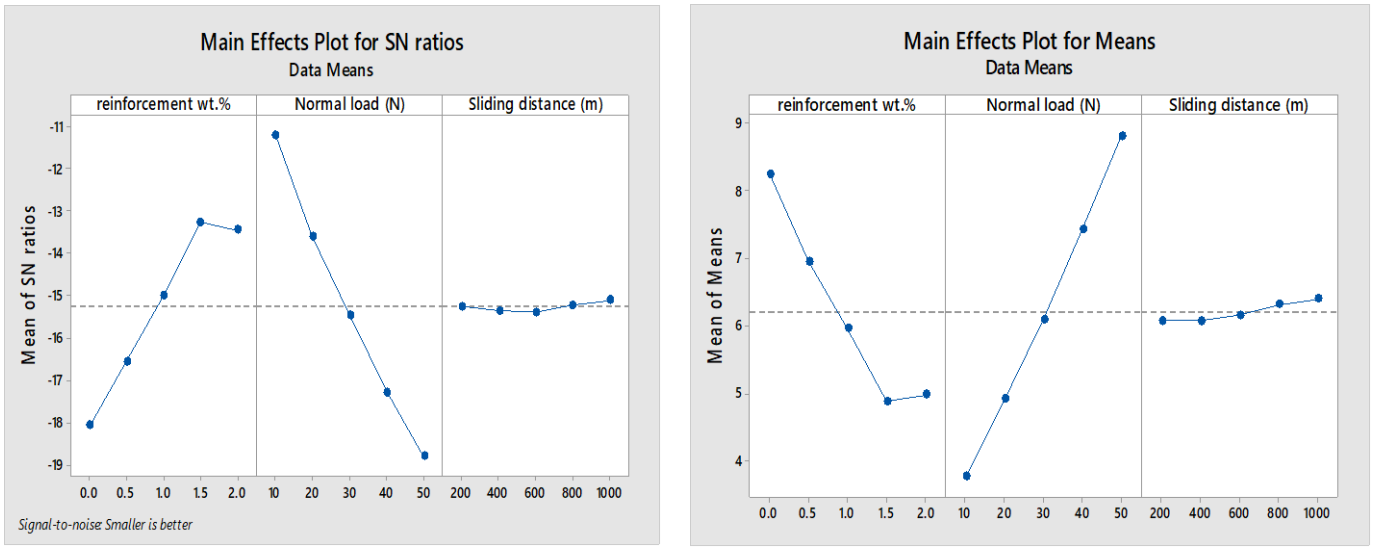

(**a**) (**b**)

Figure 9. (**a**) MEP for SN ratio (smaller is better); (**b**) MEP for means.

3.5. Analysis of Variance and Its Utility

Table 7 displays the ANOVA response for output wear loss. In this work, a 95% confidence level was selected to investigate the impact of controlling factors on wear loss. Applied (normal) load produces the maximum 65.67% contribution on wear loss from the response, while the other variable, wt.% of reinforcement, creates the second most influencing contribution of 33.23%. The third variable, sliding distance, creates a minor contribution of 0.75% on wear loss.

Table 7. Variance analysis table.

Source	DF	Seq. SS	Contribution	Ad. SS	Ad. MS	F	P
Reinforcement wt.%	4	40.505	33.23%	40.5054	10.1263	133.52	0.000
Normal load (N)	4	80.044	65.67%	80.0442	20.0110	263.84	0.000
Sliding distance (m)	4	0.425	0.35%	0.4250	0.1062	1.40	0.292
Error	12	0.910	0.75%	0.9101	0.0758		
Total	24	121.885	100.00%				

During the wear test, it is observed that the wear loss increases with applied load for all compositions due to the increased penetration of hard surface asperities to the softer surface (sample pins) with an increase in load. In addition, the softer surface asperities might be plastically deformed and fractured at higher loads, leading to material transfer between the contacting surfaces by increased temperature, resulting in higher wear loss [31].

The wear resistance increased with Si_3N_4 incorporation in AA7068 alloy from 0.5 to 1.5 wt.%. Si_3N_4 is a ceramic material with very high hardness and load-bearing capacity. When these hard particles are added to the alloy, they act as a secondary phase and resist plastic deformation. As a result, there is significant improvement in microhardness and

wear resistance of nanocomposites. Archard Equation (2) explains the relation between hardness and wear loss.

$$W = K \frac{PL}{H} \quad (2)$$

where K is a constant (dimensionless), P is applied normal load, L is sliding distance, and H is the hardness of the material. Therefore, from Equation (1), as the hardness of the material increases, the wear loss decreases. In addition, Si_3N_4 is also reactive to the surrounding humidity [8], so the SiO_2 layer formed between the interacting surfaces decreases the frictional coefficient and increases wear resistance.

Whereas, the wear loss increases for 2 wt.% nanocomposites attributed to decreased hardness and Archard Equation (2) also support wear increment when hardness decreases. In addition, the increased void content, casting defects, and particle agglomeration also contribute to wear loss increment. The mixing of nanoparticles at higher weight% is complex due to the high surface area and density difference of Al alloy and reinforcement. Nanoparticles are associated with high surface energy, and their tendency to agglomeration is relatively high, so the formation of clusters starts in various regions. As per the abovementioned facts, average microhardness and wear resistance decrease for AA7068/2 wt.% nanocomposite.

Percentage contribution directly relates to the influence of a particular variable on wear loss; the higher the contribution of the parameter, the higher the F values. The greater F values for a particular variable explain its significant influence on response; conversely, its lower values show lower impact: the *p*-value for two variables, namely reinforcement wt.% and normal load, are less than 0.05, which indicates its 5% level of significance.

In contrast, the remaining sliding distance has a more significant *p*-value, indicating insignificance. From the model summary (Table 8), adjusted R-Sq is 98.51%. The adjusted R-Sq value expresses the response variation in percentage obtained from the regression tool [36].

Table 8. Model summary.

S	R-sq	R-sq (adj)	PRESS	R-sq (pred)
0.275398	99.25%	98.51%	3.95021	96.76%

It is forecasted that the deviation in the experimental wear loss values is a function of all considered controlling variables within the range measured in the present work. Figure 10 shows the interaction plot of wear loss for all controlling factors. Referring to Figure 10, wear loss lines concerning all parameters are non-parallel. These lines indicated the interaction between control factors. The decrement in wear loss was noticed with increasing reinforcement percent up to 1.5%; after it increases, this might be credited to severe clustering/agglomeration of nanoparticles. Wear loss line for 2% is intersecting with others. By analyzing the other lines in the interaction plot, it can be concluded that the applied load has minimum interaction. The weight % and sliding distance have higher interaction than normal load; as the interaction is higher, its influence on wear loss is lower. Parveen A et al. [37] performed a dry rubbing wear test on Al/Si_3N_4 composites with various loads (20 N, 30 N, and 40 N) and sliding distances (1 km, 2 km, and 3 km). They investigated that load is the primary parameter affecting wear rate as the normal force increases the wear rate. Miloradović N et al. [38] conducted research on wear performance on ZA27/SiC/Gr composites and optimized, by the Taguchi model, different loads (10 N, 20 N, and 30 N) and sliding velocities (0.25 m/s, 0.5 m/s, and 1 m/s) that were chosen for the wear test. They observed that load has a dominant impact on wear.

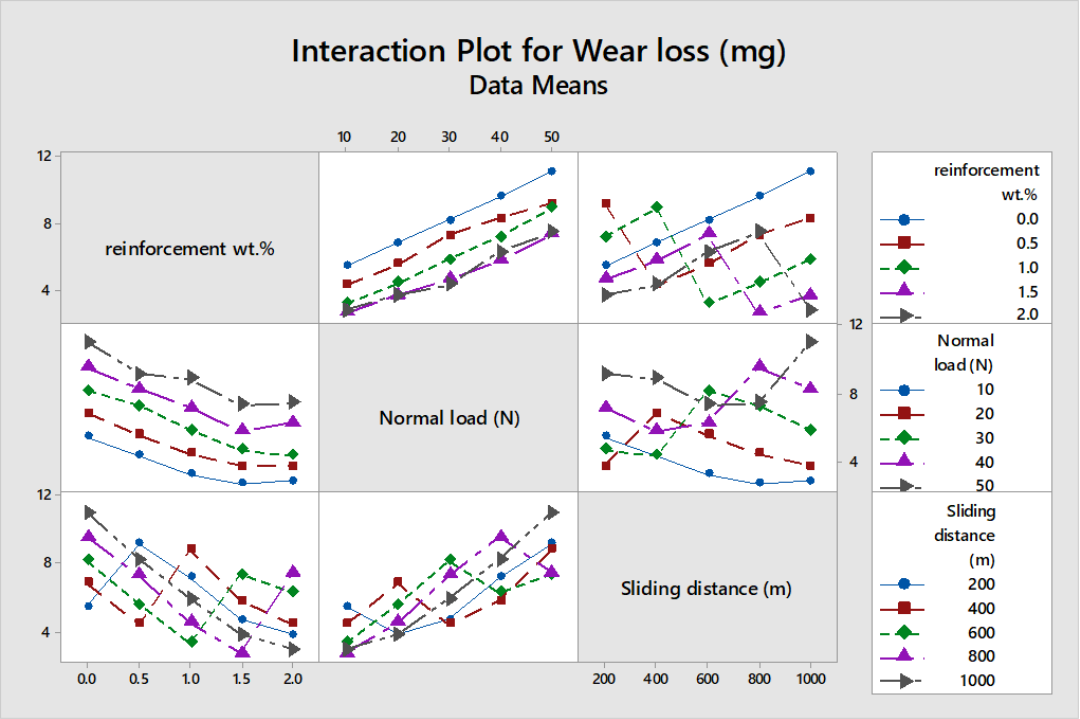

Figure 10. Interaction plot.

3.6. Regression Modeling

The relationship between response and controlling parameters is described by obtained regression Equation (2).

$$\text{Wear loss (mg)} = (2.0018 - 0.3489\ W + 0.02595\ L + 0.000032\ D)^2 \quad (3)$$

where W is the reinforcement wt.%, L is the normal load in N, and D is the rubbing distance in meters. The expected (predicted) wear loss can be calculated using Equation (3). Experimental (actual) predicted values of wear loss are shown in the L-25 matrix (Table 4). The difference in the experimental and predicted value of wear loss is known as residual (error).

Consequently, versus fits curve/scatter plots, where residuals are on the vertical axis and expected data are on the horizontal axis, explain the non-linearity, unlike error variance. From the normal probability graph, maximum data are fitted near or on the line that explains the accuracy of the predicted value calculated by Equation (3). In addition, the x- and y-axes are approximately symmetrical, showing that obtained results are significantly modeled and accurate. The unevenness of factors in all residual graphs is uniform over the range of formulated values. From the above discussion, it can be concluded that the current regression model is the best fit to explicate the present study's observed data. The comparison between actual and formulated wear loss for each experiment displayed in Table 4 is shown in Figure 11.

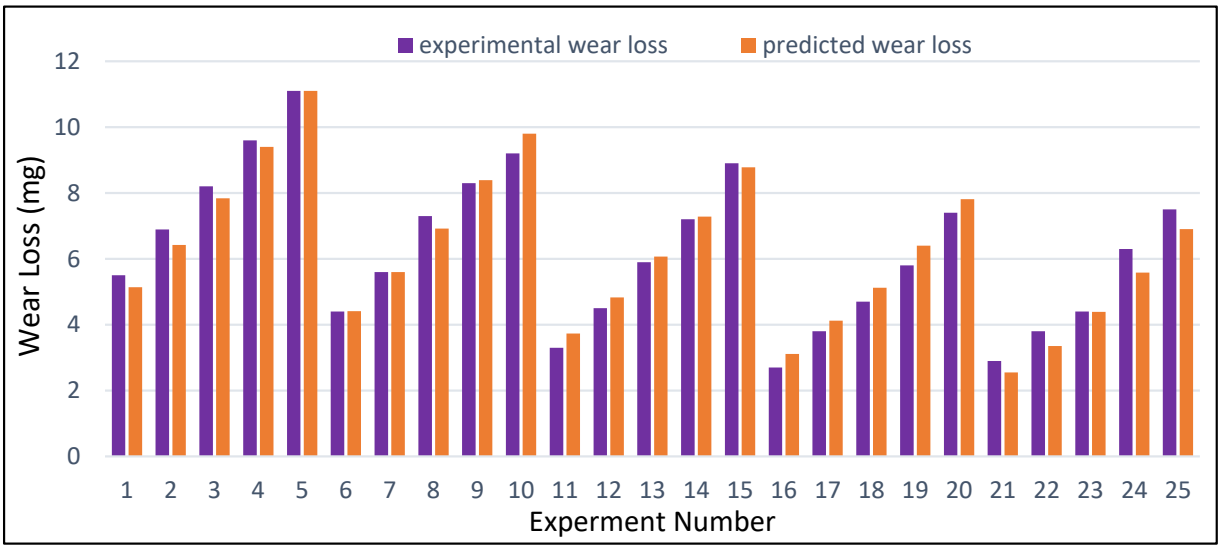

Figure 11. Actual versus formulated (predicted) wear loss for each run.

Similarly, the residual curve for wear loss (shown in Figure 12) further interprets the actual wear and formulated (predicted) wear. The histogram plot for wear loss explains the residual range from −0.12 to 0.16. As per this histogram, the maximum frequency obtained at zero residual is evidence of the regression equation's best fit observed data model (2).

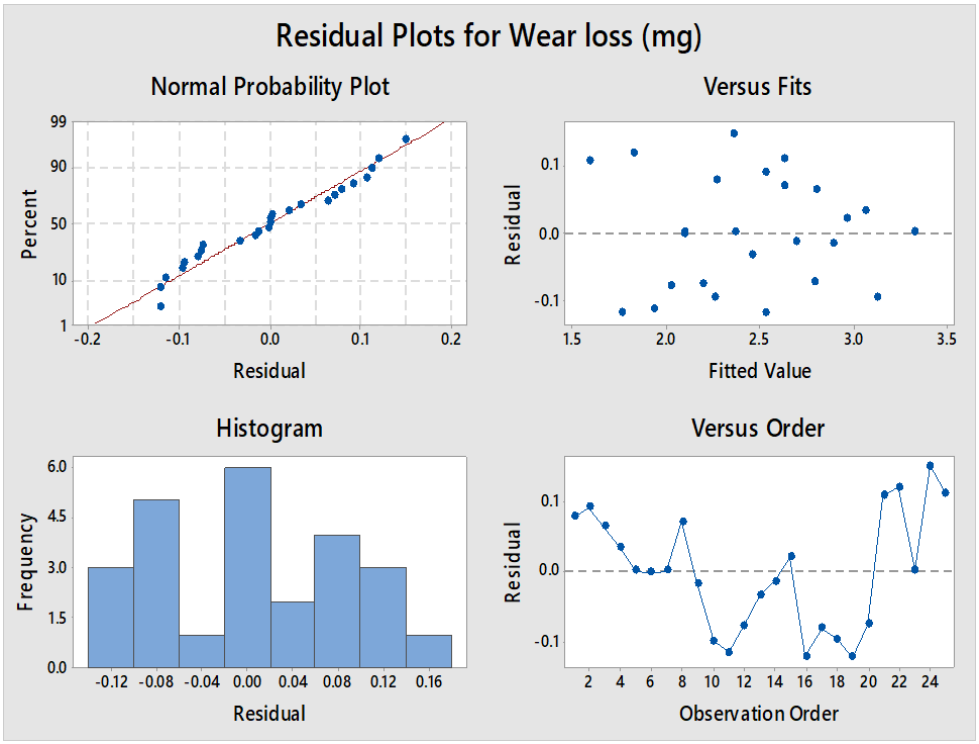

Figure 12. Residual graphs for wear loss.

3.7. Confirmation Experiment

The main objective of this work is to optimize the wear loss to improve the quality of AA7068/Si_3N_4 nanocomposites produced by ultrasonic-assisted casting. Referring to Equation (1), SNR shows negative logarithmic dependency on wear rate, which should be maximized to obtain optimum values. Therefore, for each factor, the maximized value provides the optimum level. From Tables 5 and 6, it is recognized that the optimum levels

for each factor are 1.5 wt.% reinforcement, 10 N normal load, and 400 m sliding distance. It can be observed that the minimum wear loss would be obtained with optimum values. Table 9 displayed confirmation test results; the average experimental wear loss measured 3.214 mg (by taking an average of five test results) after performing a wear test on optimum values of control factors that are smaller than other combinations.

Table 9. Optimized values and confirmation test.

			Wear Loss (mg)			
Control Variables	**Optimized Value**	**Test No.**	**Experimental**	**Predicted**	**Error (%)**	**SNR**
Reinforcement wt.%	1.5	1	2.45		−25.10	
Load (N)	10	2	2.21	3.065	−38.68	−8.530
Sliding distance (m)	400	3	3.11		1.44	
		4	2.73		−12.27	
		5	2.86		−7.16	
		Average	2.67	3.065	−14.79	−8.530

3.8. Contour and Surface Plots

Contour plots are two-dimensional representations, where the third z-axis is constant and named as a contour while the x- and y-axes are visible. Surface plots are three-dimensional layouts where all three axes are visible. This study draws contour and surface plots to understand the expected link between three process variables. Figure 13a–f shows the contour and surface graphs of wear loss versus process variables (reinforcement wt.%, normal load, and sliding distance); all the plots are drawn by considering two control factors. The dark green area in contour plots depicts the significant wear loss. A conversion from light green to dark green directly expresses the wear loss from low to high. From Figure 13a,b, higher wear loss can be seen at a higher load (40 N, 50 N) and low concentration, with minimum wear obtained at 1.5 wt.% and an increase again at 2 wt.%. Figure 13c,d explains that the wear increases with sliding distance, but for low concentrations (0 and 0.5), as the second phase increases in the matrix, wear loss is not much enhanced with sliding distance. As per the study of sliding wear of AA7075/SiC composites at different sliding distances, a more significant wear rate was found for alloy and decreased with increasing concentration of SiC (0.5 to 2 wt.%) [1]. Figure 13e,f shows low wear loss found at low load and less distance, but it enhances when the load increases from 10 N to 50 N. Kumar GBV et al. [35] noticed the increased weight loss with an increment in load from 10 N to 60 N in Al 6063/Si_3N_4 composites. From the contour and surface plot analysis, it can be concluded that load is the major parameter that influences wear loss, followed by wt.% and sliding distance as minor influential factors.

3.9. Worn Surface Study

Worn surface characterization of composites is more complex than alloys and metals. The SEM study of the worn surface was carried out to examine the dominant wear mechanism in the Al matrix and their nanocomposites at different weight % of Si_3N_4. The SEM micrographs of AA7068 alloy and nanocomposites at 50 N applied load and 1.047 m/s sliding velocity for a 1000 m sliding distance are shown in Figure 14. Figure 14a represents the worn surface of AA7068, and a severe plastically deformed and delaminated surface was observed. At the beginning of the wear test, the asperities of the specimen pin and counter disc came under contact. The counter surface distorted softer surface asperities during the initial stage of sliding action. Further sliding leads to the formation and breaking of junctions at the interface under high pressure, leading to plastic deformation of a softer surface. The material transfer also starts between interacting surfaces due to the temperature rise by the action of friction.

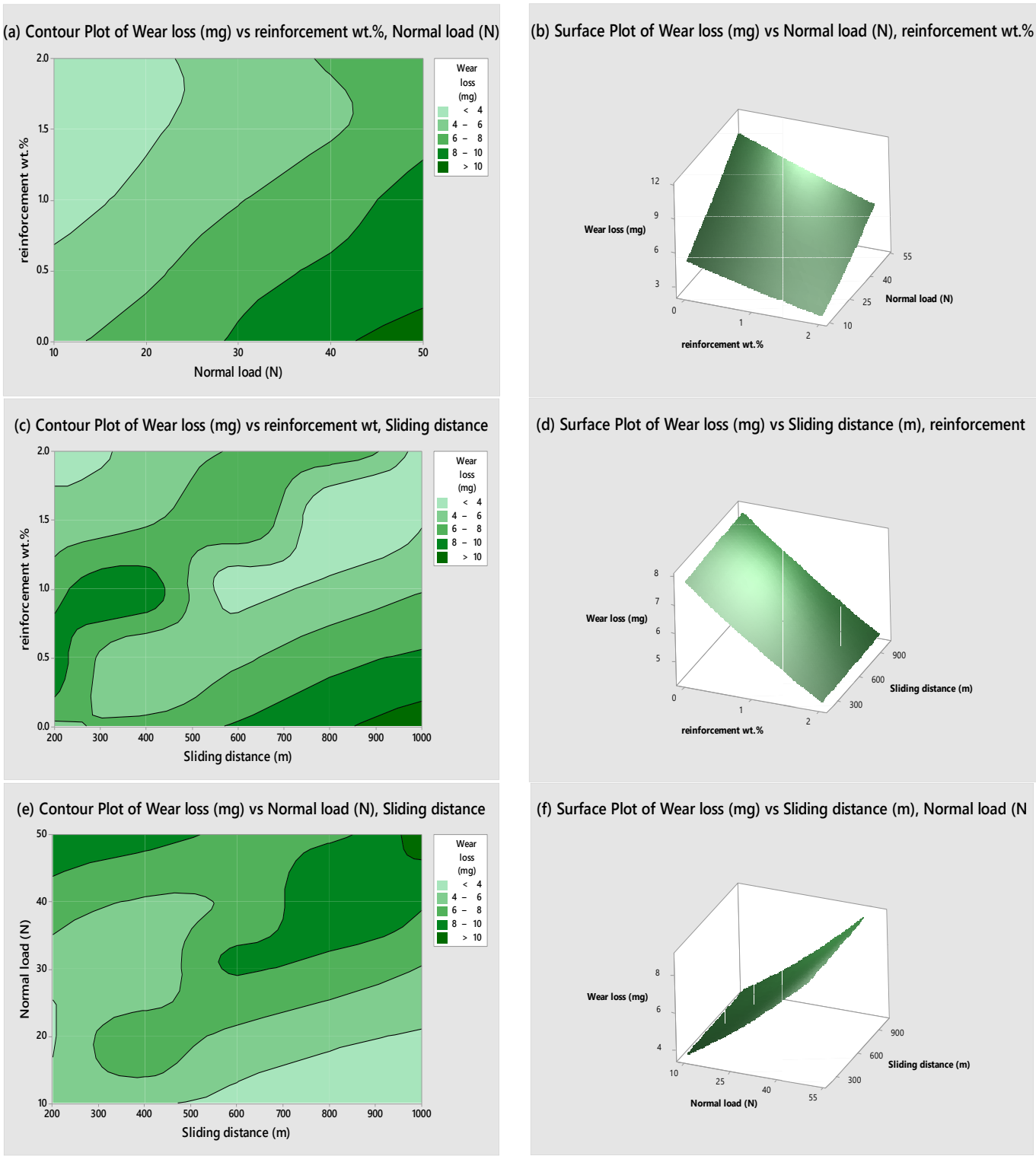

Figure 13. (**a**,**c**,**e**) Contour plots, (**b**,**d**,**f**) surface plots, of wear rate versus all combinations of reinforcement wt.%, sliding distance (m), and normal load (N).

Meanwhile, the worn surface of nanocomposites is smoother than matrix alloy. Finer grooves were observed in micrographs of nanocomposites compared to AA7068 (shown in Figure 14b–e, attributed to the increased wear resistance after the inclusion of hard Si_3N_4 nanoparticles in AA7068. In addition, Si_3N_4 is also reactive to the surrounding humidity: it reacts with atmospheric H_2O and forms a SiO_2 layer between the contacting interface.

This oxide layer prevents the direct contact of the specimen with the hard counter disc. It acts as a lubricant, resulting in decreasing the coefficient of friction and increasing wear resistance. Moreover, it is evident from Figure 14d that the grooves are closely packed and much smaller in AA7068/1.5 wt.% Si_3N_4 nanocomposite due to the sliding action of a large number of hard Si_3N_4 particles and debris. However, it is observed that the wear loss increased after 1.5 wt.% due to the increased porosity and ununiform distribution of reinforcing particles. Pits and the crumbled region observed in the micrograph of AA7068/2 wt.% Si_3N_4 nanocomposites (shown in Figure 14e) support increased wear loss due to high void content, casting defects, agglomeration, and material spallation. The cluster of particles improves the wear resistance at lower, medium load, and sliding distances due to the hard nature of Si_3N_4 particles and tribo-chemical layers (MML) formation between the contacting surfaces, resulting in wear resistance improvement. However, as the load and distance increased, the formed MML deformed due to a rise in temperature, material softening, and material transfer, leading to a decrease in wear resistance. In addition, higher-degree three-body abrasion by wear debris, material spallation, and Archard equation support the increase in wear loss for 2 wt.% nanocomposites.

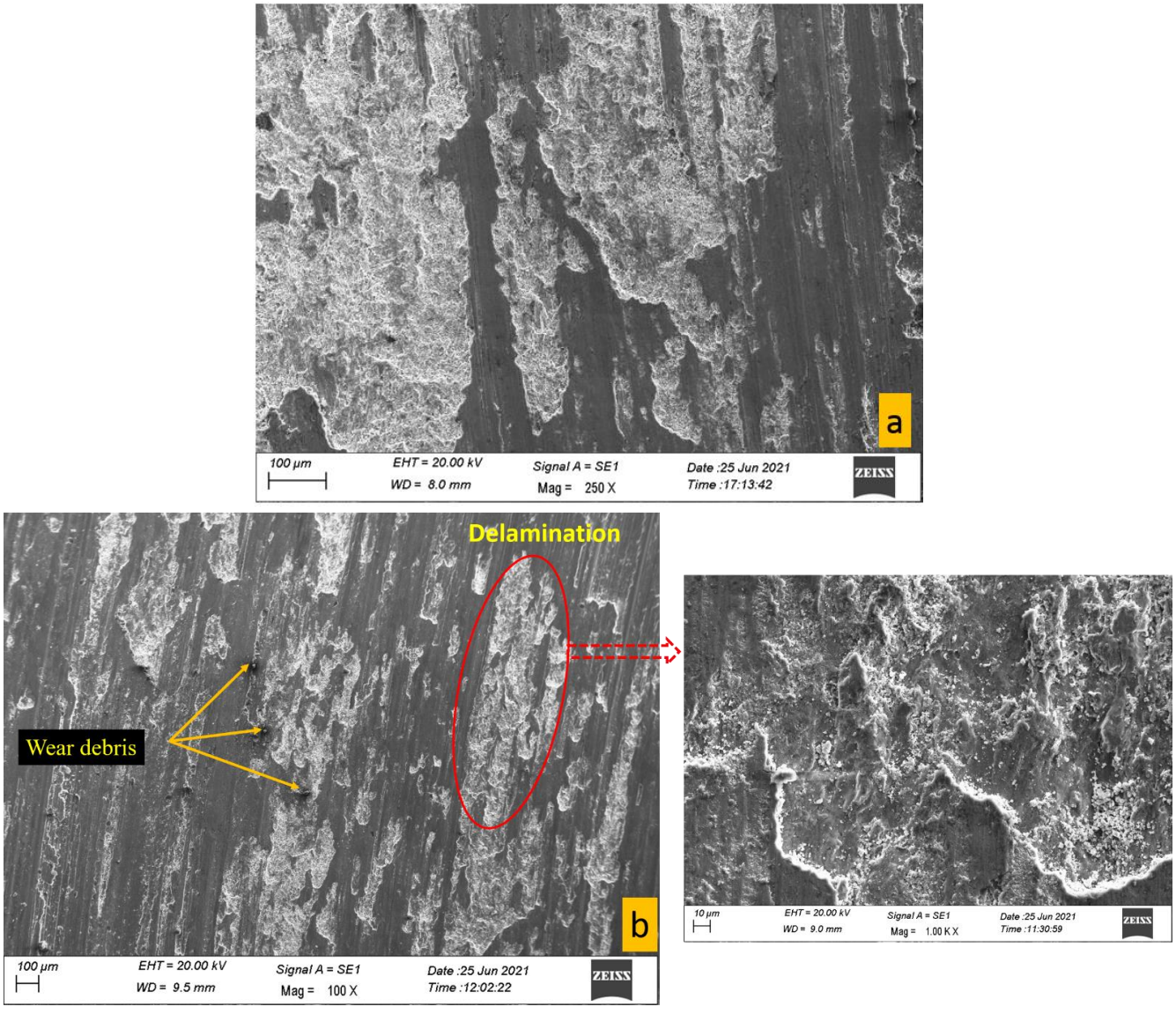

Figure 14. *Cont.*

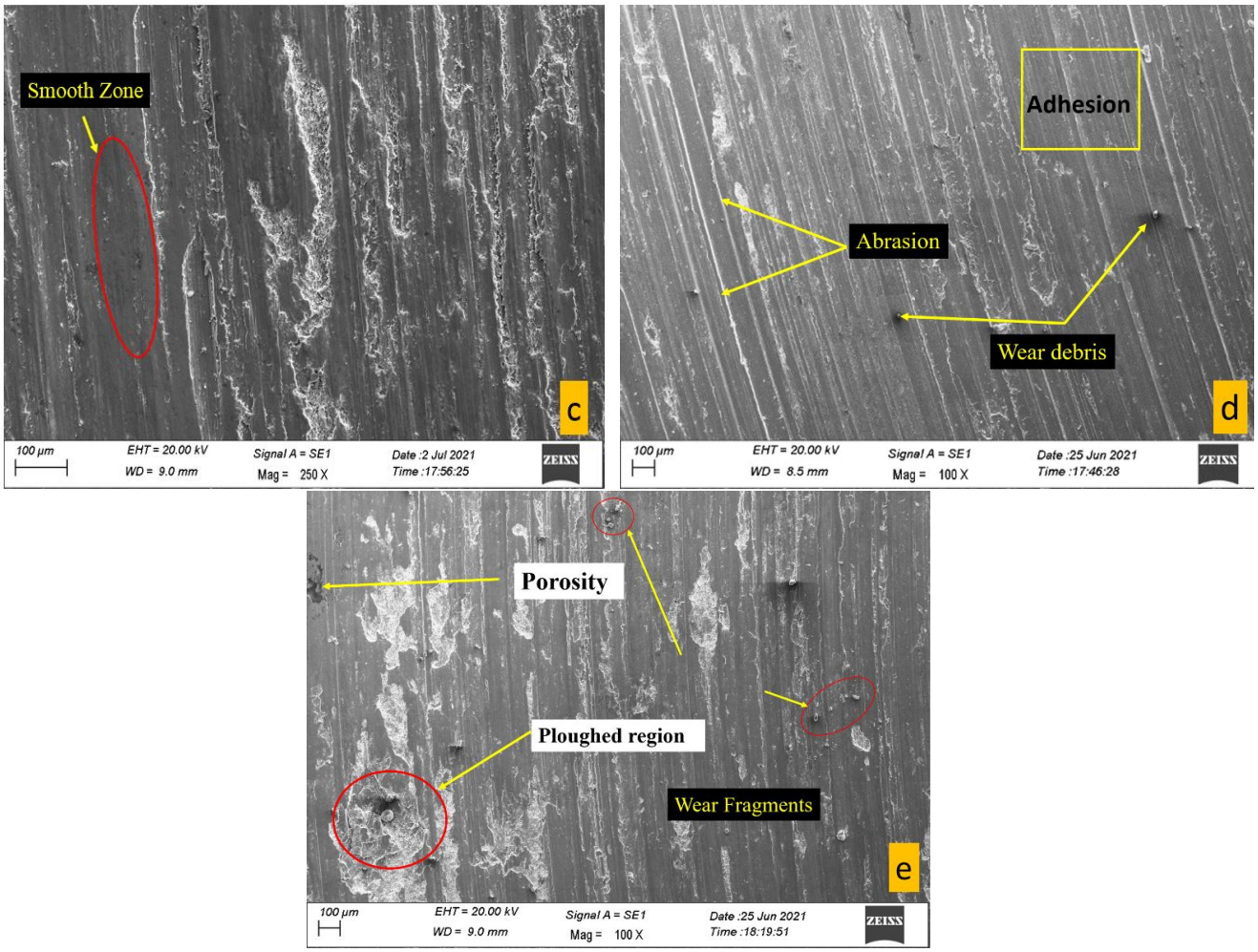

Figure 14. Worn surface SEM micrographs at 50 N normal load, 1000 m sliding distance, and 1.047 m/s sliding velocity: (**a**) Al alloy 7068; (**b**) AA7068/0.5wt.% Si_3N_4; (**c**) AA7068/1.0 wt.% Si_3N_4; (**d**) AA7068/1.5 wt.% Si_3N_4; (**e**) AA7068/2.0 wt.% Si_3N_4.

It is concluded from the worn micrograph study that abrasion is the dominating wear mechanism resulting from three-body abrasion. The secondary wear mechanism is fatigue spallation started at the alloy metallic matrix and ceramic reinforcement interfaces and adhesive smearing of nanocomposites.

Figure 15 shows the elemental mapping of the worn surface of the nanocomposite, where the presence of major elements in AMNC, such as Al, Zn, Cu, Mg, Si, and N, are confirmed and shown with different colors.

Figure 16 represents EDS of 0.5 wt.% nanocomposites at 40 N load after a run of 800 m. The observed elemental information with weight % is shown in the table (inside the EDS plot). The presence of oxygen indicates oxidation at the surface during sliding wear.

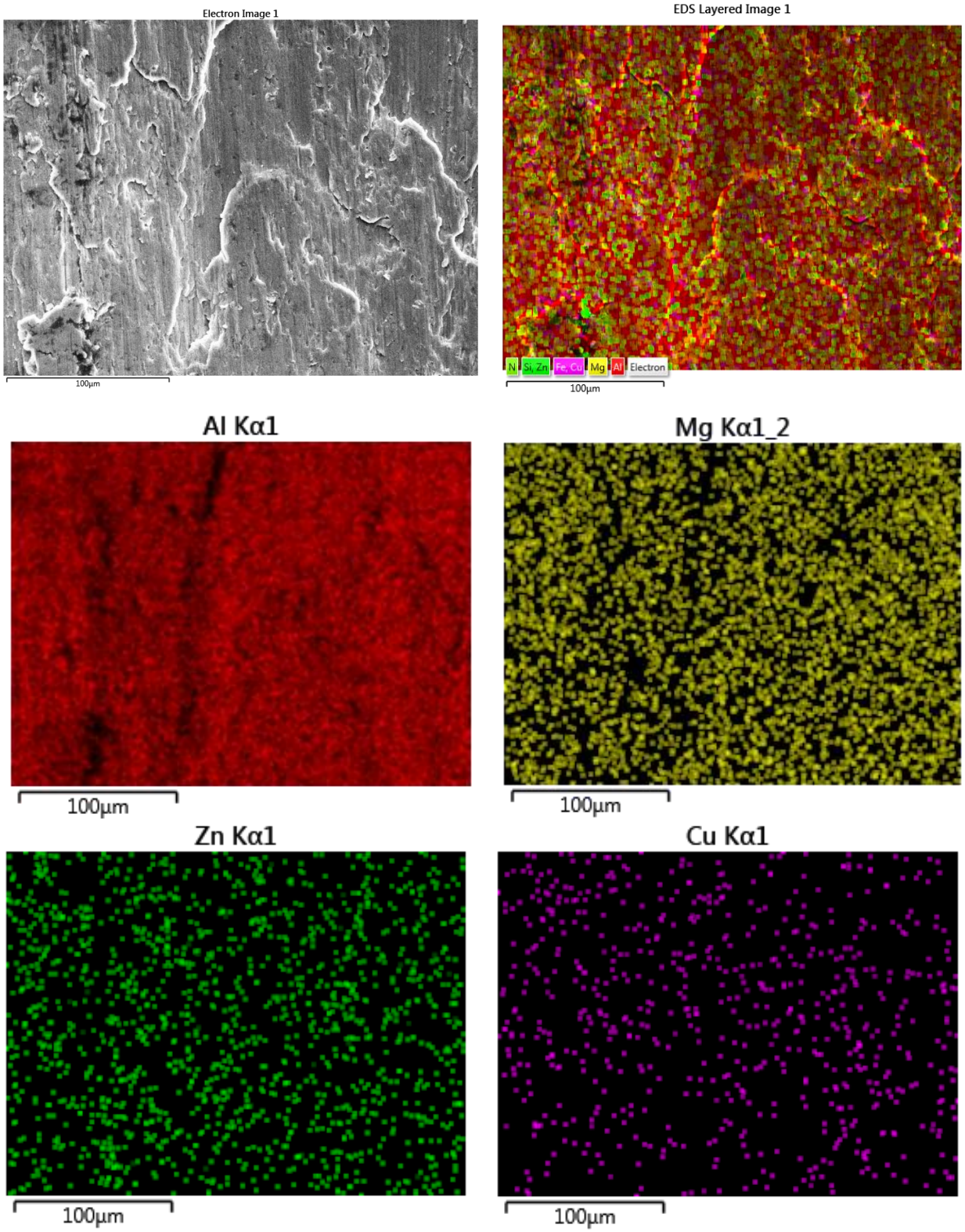

Figure 15. *Cont.*

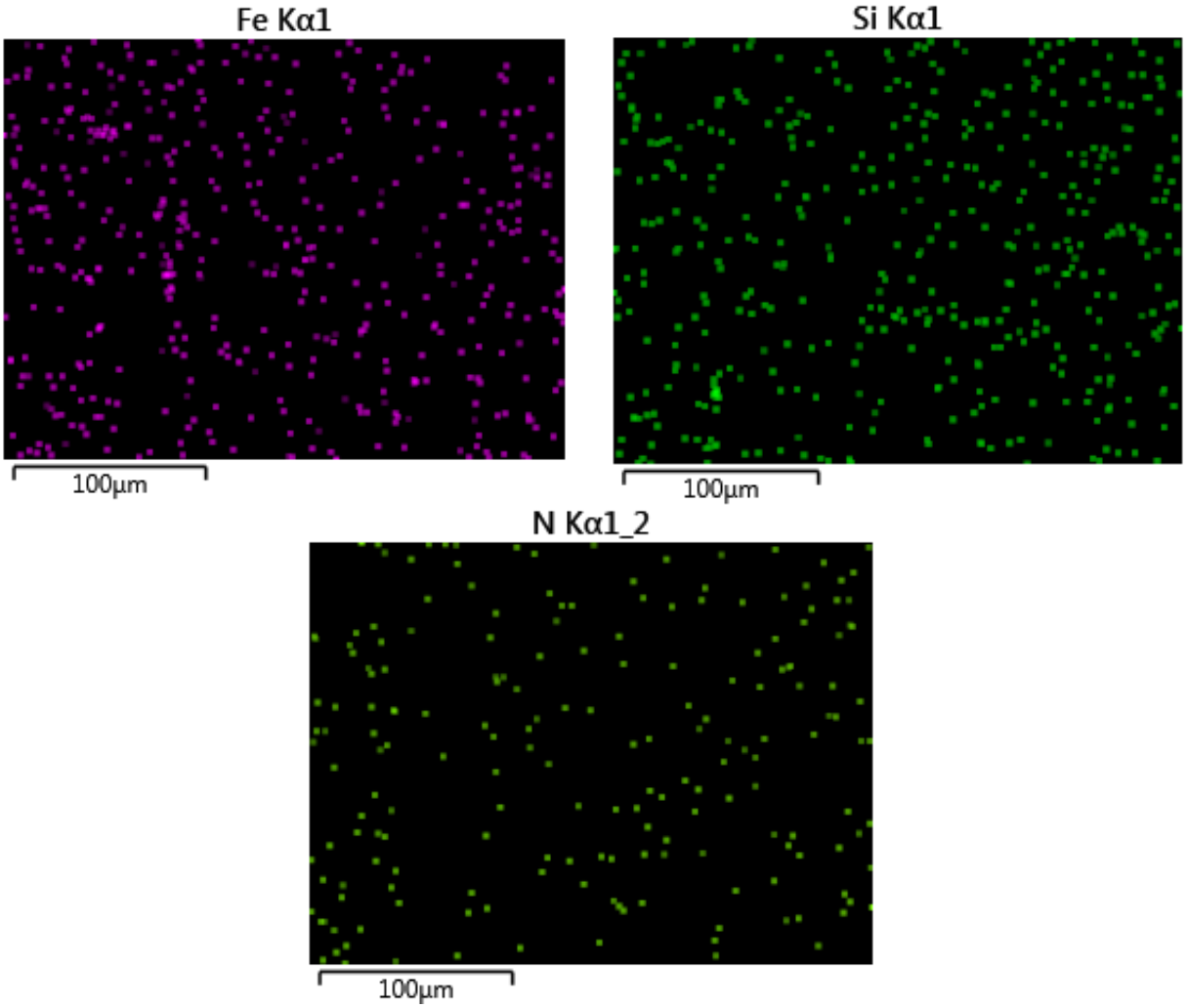

Figure 15. Elemental mapping of worn surface of 0.5 wt.% nanocomposite.

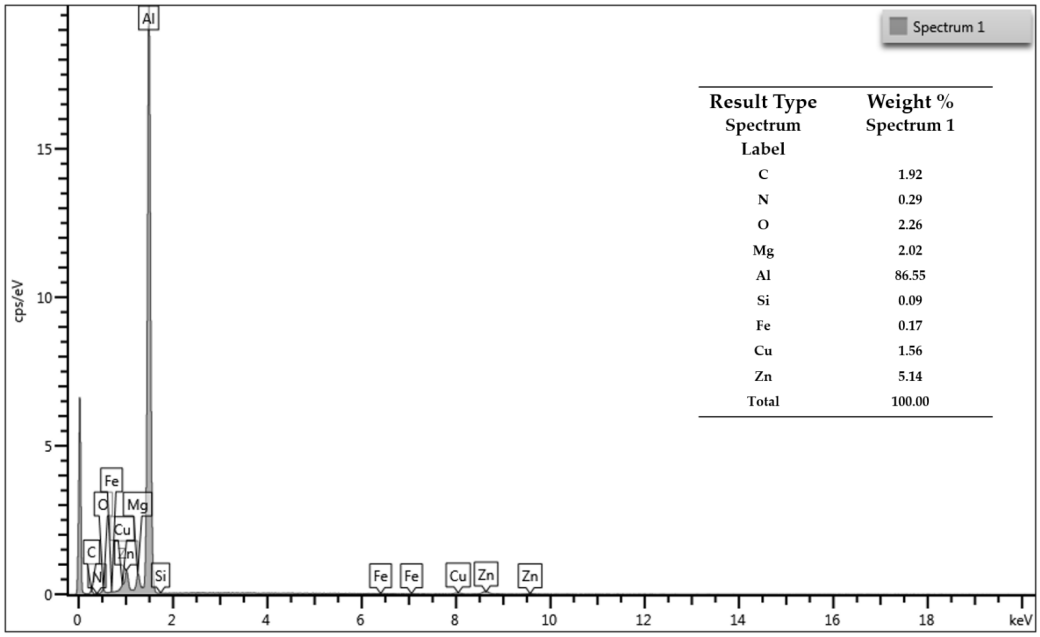

Figure 16. Worn surface EDS for 0.5 wt.% nanocomposite at 40 N load and 800 m sliding distance.

4. Conclusions

Production of (Si_3N_4)np reinforced AA7068 alloy composites was successfully completed through stir casting combined with ultrasonication, followed by bottom pouring in a steel mold. Nanocomposites were fabricated with a different fraction of Si_3N_4 (0.5, 1, 1.5, and 2%) by weight.

1. The FESEM results revealed the presence of Si_3N_4 particles in the alloy, and reinforcement is homogeneously dispersed in the matrix alloy from 0.5 to 1.5 wt.%. In contrast, agglomeration of fine particles was found in nanocomposites reinforced with 2 wt.% Si_3N_4.
2. From the microstructure analysis, α-Al and η-$MgZn_2$ eutectic phases were observed in cast 7068 aluminum alloy, and coarse grains of the matrix were significantly refined with the incorporation of Si_3N_4 nanoparticles.
3. Improvement in hardness was noticed up to 1.5 wt.%, and it reduced at 2 wt.% due to the clustering of particles. The hardness of the alloy significantly increased (32.72%) with the addition of 1.5 wt.% Si_3N_4 due to the combined effect of uniform dispersion of nanoparticles and increased load-bearing capacity by Si_3N_4.
4. Normal load produces the highest percent contribution, 65.67%, on wear loss; wt.% of reinforcement creates the second most influencing contribution of 33.23%, and a minor contribution was noticed for sliding distance.
5. The optimum levels of each factor are 1.5 wt.% Si_3N_4 reinforcement, 10 N normal load, and 400 m sliding distance. The confirmation wear test observed a minimum wear loss of 2.67 mg on optimum parameters.
6. It is observed from the worn micrograph study that abrasion is the dominating wear mechanism resulting from three-body abrasion. The secondary wear mechanism is fatigue spallation started at the alloy metallic matrix and ceramic reinforcement interfaces and adhesive smearing of nanocomposites.

Author Contributions: Conceptualization, A.K., R.P. and R.S.R.; methodology, A.K., R.P. and R.S.R.; software, A.K., K.K.S. and J.X.; formal analysis, J.X., V.M. and A.K.; investigation, A.K. and R.S.R.; resources, R.P., V.M., K.K.S. and J.X.; data curation, R.P., R.S.R. and A.K.; writing—original draft preparation, R.S.R. and A.K.; writing—review and editing, K.K.S., J.X., V.M., R.S.R. and A.K.; visualization, K.K.S. and V.M.; supervision, R.P. and R.S.R.; project administration, R.S.R. and R.P. All authors have read and agreed to the published version of the manuscript.

Funding: This research received no external funding.

Institutional Review Board Statement: Not applicable.

Informed Consent Statement: Not applicable.

Data Availability Statement: Not applicable.

Acknowledgments: The authors would like to extend their thanks and appreciation to MSE Dept. IIT Kanpur and MSME Dept. MANIT, Bhopal, India for the provision of characterization facilities.

Conflicts of Interest: The authors declare no conflict of interest.

References

1. Rao, T.B. Microstructural, mechanical, and wear properties characterization and strengthening mechanisms of Al7075/SiCnp composites processed through ultrasonic cavitation assisted stir-casting. *Mater. Sci. Eng. A* **2020**, *805*, 140553. [CrossRef]
2. Ghandvar, H.; Farahany, S.; Idris, J. Wettability Enhancement of SiCp in Cast A356/SiCp Composite Using Semisolid Process. *Mater. Manuf. Process.* **2015**, *30*, 1442–1449. [CrossRef]
3. Srivastava, N.; Chaudhari, G. Strengthening in Al alloy nano composites fabricated by ultrasound assisted solidification technique. *Mater. Sci. Eng. A* **2016**, *651*, 241–247. [CrossRef]
4. Mistry, J.M.; Gohil, P.P. Experimental investigations on wear and friction behaviour of Si3N4p reinforced heat-treated aluminium matrix composites produced using electromagnetic stir casting process. *Compos. Part B Eng.* **2018**, *161*, 190–204. [CrossRef]

5. Chen, Z.; Sun, G.; Wu, Y.; Mathon, M.; Borbely, A.; Chen, D.; Ji, G.; Wang, M.; Zhong, S.; Wang, H. Multi-scale study of microstructure evolution in hot extruded nano-sized TiB 2 particle reinforced aluminum composites. *Mater. Des.* **2017**, *116*, 577–590. [CrossRef]
6. Sheelwant, A.; Dutta, S.; Sonti, K.S.M.; Narala, S.K.R. Processing and performance assessment of particulate TiB2 reinforced aluminum MMC developed via a novel hybrid ultrasonic casting system. *Mater. Manuf. Process.* **2021**, *37*, 186–196. [CrossRef]
7. Zhou, D.; Qiu, F.; Jiang, Q. The nano-sized TiC particle reinforced Al–Cu matrix composite with superior tensile ductility. *Mater. Sci. Eng. A* **2015**, *622*, 189–193. [CrossRef]
8. Sivaraj, M.; Selvakumar, N. Experimental Analysis of Al–TiC Sintered Nanocomposite on EDM Process Parameters Using ANOVA. *Mater. Manuf. Process.* **2015**, *31*, 802–812. [CrossRef]
9. Joshua, K.J.; Vijay, S.; Selvaraj, D.P. Effect of nano TiO2 particles on microhardness and microstructural behavior of AA7068 metal matrix composites. *Ceram. Int.* **2018**, *44*, 20774–20781. [CrossRef]
10. Alipour, M.; Eslami-Farsani, R. Synthesis and characterization of graphene nanoplatelets reinforced AA7068 matrix nanocomposites produced by liquid metallurgy route. *Mater. Sci. Eng. A* **2017**, *706*, 71–82. [CrossRef]
11. Chak, V.; Chattopadhyay, H.; Dora, T.L. Application of solid processing routes for the synthesis of graphene-aluminum composites—A review. *Mater. Manuf. Process.* **2021**, *36*, 1219–1235. [CrossRef]
12. Turan, M.E.; Aydin, F.; Sun, Y.; Zengin, H.; Akinay, Y. Wear resistance and tribological properties of GNPs and MWCNT reinforced AlSi18CuNiMg alloys produced by stir casting. *Tribol. Int.* **2021**, *164*, 107201. [CrossRef]
13. Prakash, C.; Senthil, P.; Manikandan, N.; Palanisamy, D. Investigations on machinability characteristics of Cast Aluminum Alloy based (LM 26+Graphite+Fly ash) Hybrid Metal Matrix Composites for automobile components. *Mater. Manuf. Process.* **2022**, *137*, 748–763. [CrossRef]
14. Madhusudhan, M.; Naveen, G.; Mahesha, K. Mechanical Characterization of AA7068-ZrO 2 reinforced Metal Matrix Composites. *Mater. Today Proc.* **2017**, *4*, 3122–3130. [CrossRef]
15. Etemadi, R.; Wang, B.; Pillai, K.M.; Niroumand, B.; Omrani, E.; Rohatgi, P. Pressure infiltration processes to synthesize metal matrix composites—A review of metal matrix composites, the technology and process simulation. *Mater. Manuf. Process.* **2018**, *33*, 1261–1290. [CrossRef]
16. Kumar, N.; Gautam, G.; Gautam, R.K.; Mohan, A.; Mohan, S. A Study on Mechanical Properties and Strengthening Mechanisms of AA5052/ZrB2 In Situ Composites. *J. Eng. Mater. Technol.* **2016**, *139*, 011002. [CrossRef]
17. Basumallick, A.; Ghosh, S. Processing of In Situ Aluminium Matrix Composites by Micropyretic Reactive Sintering. *Mater. Manuf. Process.* **2007**, *22*, 692–695. [CrossRef]
18. Bajakke, P.; Malik, V.; Deshpande, A.S. Particulate metal matrix composites and their fabrication via friction stir processing—A review. *Mater. Manuf. Process.* **2019**, *34*, 833–881. [CrossRef]
19. Winnicki, M.; Malachowska, A.; Piwowarczyk, T.; Rutkowska-Gorczyca, M.; Ambroziak, A. The bond strength of Al+Al2O3 cermet coatings deposited by low-pressure cold spraying. *Arch. Civ. Mech. Eng.* **2016**, *16*, 743–752. [CrossRef]
20. Ghassemieh, E. Materials in Automotive Application, State of the Art and Prospects. *New Trends Dev. Automot. Ind.* **2011**, *20*, 365–394. [CrossRef]
21. Srivastava, N.; Chaudhari, G. Microstructural evolution and mechanical behavior of ultrasonically synthesized Al6061-nano alumina composites. *Mater. Sci. Eng. A* **2018**, *724*, 199–207. [CrossRef]
22. Chak, V.; Chattopadhyay, H. Fabrication and heat treatment of graphene nanoplatelets reinforced aluminium nanocomposites. *Mater. Sci. Eng. A* **2020**, *791*, 139657. [CrossRef]
23. Tavoosi, M.; Karimzadeh, F.; Enayati, M.; Heidarpour, A. Bulk Al–Zn/Al2O3 nanocomposite prepared by reactive milling and hot pressing methods. *J. Alloys Compd.* **2009**, *475*, 198–201. [CrossRef]
24. Yuan, D.; Yang, X.; Wu, S.; Lü, S.; Hu, K. Development of high strength and toughness nano-SiCp/A356 composites with ultrasonic vibration and squeeze casting. *J. Mater. Process. Technol.* **2019**, *269*, 1–9. [CrossRef]
25. Yigezu, B.S.; Jha, P.K.; Mahapatra, M.M. The Key Attributes of Synthesizing Ceramic Particulate Reinforced Al-Based Matrix Composites through Stir Casting Process: A Review. *Mater. Manuf. Process.* **2013**, *28*, 969–979. [CrossRef]
26. Lan, J.; Yang, Y.; Li, X. Microstructure and microhardness of SiC nanoparticles reinforced magnesium composites fabricated by ultrasonic method. *Mater. Sci. Eng. A* **2004**, *386*, 284–290. [CrossRef]
27. Hu, K.; Yuan, D.; Lü, S.-L.; Wu, S.-S. Effects of nano-SiCp content on microstructure and mechanical properties of SiCp/A356 composites assisted with ultrasonic treatment. *Trans. Nonferrous Met. Soc. China* **2018**, *28*, 2173–2180. [CrossRef]
28. Yang, X.; Wu, S.; Lü, S.; Hao, L.; Fang, X. Refinement of LPSO structure in Mg-Ni-Y alloys by ultrasonic treatment. *Ultrason. Sonochemistry* **2018**, *40*, 472–479. [CrossRef]
29. Yang, Y.; Lan, J.; Li, X. Study on bulk aluminum matrix nano-composite fabricated by ultrasonic dispersion of nano-sized SiC particles in molten aluminum alloy. *Mater. Sci. Eng. A* **2004**, *380*, 378–383. [CrossRef]
30. Mohanavel, V.; Ali, K.A.; Prasath, S.; Sathish, T.; Ravichandran, M. Microstructural and tribological characteristics of AA6351/Si3N4 composites manufactured by stir casting. *J. Mater. Res. Technol.* **2020**, *9*, 14662–14672. [CrossRef]
31. Sharma, N.; Khanna, R.; Singh, G.; Kumar, V. Fabrication of 6061 aluminum alloy reinforced with Si_3N_4/n-Gr and its wear performance optimization using integrated RSM-GA. *Part. Sci. Technol.* **2016**, *35*, 731–741. [CrossRef]
32. Ambigai, R.; Prabhu, S. Optimization of friction and wear behaviour of Al–Si 3 N 4 nano composite and Al–Gr–Si_3N_4 hybrid composite under dry sliding conditions. *Trans. Nonferrous Met. Soc. China* **2017**, *27*, 986–997. [CrossRef]

33. Bhuvanesh, D.; Radhika, N. Experimental investigation on tribological characteristics of silicon nitride reinforced Aluminium metal matrix composites. *J. Eng. Sci. Technol.* **2017**, *12*, 1295–1306.
34. Sathish, T.; Karthick, S. Wear behaviour analysis on aluminium alloy 7050 with reinforced SiC through taguchi approach. *J. Mater. Res. Technol.* **2020**, *9*, 3481–3487. [CrossRef]
35. Kumar, G.; Panigrahy, P.P.; Nithika, S.; Pramod, R.; Rao, C. Assessment of mechanical and tribological characteristics of Silicon Nitride reinforced aluminum metal matrix composites. *Compos. Part B Eng.* **2019**, *175*, 107138. [CrossRef]
36. Veličković, S.; Stojanović, B.; Babić, M.; Bobic, I. Optimization of tribological properties of aluminum hybrid composites using Taguchi design. *J. Compos. Mater.* **2016**, *51*, 2505–2515. [CrossRef]
37. Parveen, A.; Chauhan, N.R.; Suhaib, M. Study of Si_3N_4 reinforcement on the morphological and tribo-mechanical behaviour of aluminium matrix composites. *Mater. Res. Express* **2018**, *6*, 042001. [CrossRef]
38. Miloradović, N.; Vujanac, R.; Stojanović, B.; Pavlović, A. Dry sliding wear behaviour of ZA27/SiC/Gr hybrid composites with Taguchi optimization. *Compos. Struct.* **2021**, *264*, 113658. [CrossRef]